

## Static and dynamic light scattering in nonionic critical micellar solutions of water–pentaethylene glycol *n*-dodecylether

K. Hamano, K. Fukuhara, and N. Kuwahara

*Department of Biological and Chemical Engineering, Faculty of Technology, Gunma University, Kiryu, Japan*

E. Ducros, M. Benseddik, and J. Rouch

*Centre de Physique Moléculaire Optique et Hertzienne, Université Bordeaux I, 351 Cours de la Libération, 333405 Talence, France*

P. Tartaglia

*Dipartimento di Fisica, Università di Roma La Sapienza, Piazzale Aldo Moro 2, Roma, Italy*

(Received 28 November 1994; revised manuscript received 6 March 1995)

Extensive sets of measurements of the shear viscosity, the scattered light intensity, and the relaxation rate of the order-parameter fluctuations lead us to reexamine the static and dynamic critical behaviors of binary solutions of pentaethylene glycol *n*-dodecylether ( $C_{12}E_5$ ) and water. The scattered intensity, the scattered field correlation function, and the relaxation rate of the order parameter show systematic deviations from the behavior usually observed for simple or molecular binary fluids. A modified version of the Sorensen *et al.* [Phys. Rev. A **13**, 1593 (1976)] dynamical droplet model that assumes that close to the critical point the critical clusters can be treated much like percolating aggregates having a fractal dimension  $d_f=2.49$  and an associated polydispersity exponent  $\tau=2.21$  and which includes the finite size of the micelles, very well accounts for all our experimental results.

PACS number(s): 82.70.-y, 64.70.-p, 78.20.-e

### I. INTRODUCTION

Numerous studies can be found in the literature on nonionic amphiphile alkyoxyethylene glycol monoether  $C_iE_j$  + water critical micellar solutions and in multicomponent water + oil + amphiphile mixtures, namely microemulsions [1]. These mixtures can create self-assembling microstructures, e.g., quasispherical micelles, whose sizes depend essentially on concentration and temperature. Most experimental studies in nonionic micellar systems [2–7] have shown that the static and dynamical critical behaviors can be interpreted in terms of critical-point universality [8], where the critical exponents and the associated scaling functions describing the divergence of the relevant physical quantities are identical to those expected for a pure fluid or a binary mixture belonging to the same three-dimensional (3D) Ising universality class. However, in some of these critical mixtures forming micelles like  $C_{12}E_5 + H_2O$ , the exponents  $\gamma$  and  $\nu$ , characterizing the divergence of the osmotic compressibility  $\chi_T$  and of the long-range correlation length  $\xi$ , are found to be apparently smaller than the corresponding universal 3D Ising estimates [2,9,10]. These experimental results have been the source of a number of theoretical works on the subject, giving plausible arguments for a possible nonuniversal behavior [11–13]. Bearing in mind that the micelle itself has a rather “soft” structure in the sense that micelles are dynamic entities which are continuously and reversibly exchanging monomers with one another, it has been argued that growth and conformational changes of the individual micelles should be taken into account as the temperature and the concentration are modified [14].

This salient feature of micellar aggregates may appear in significant morphological changes induced by varying the total surfactant concentration, temperature, ionic strength, and other physical conditions [15]. Another approach [16] was to consider the effect on the critical dynamics of the background terms of the transport coefficients, in this case mutual diffusion and shear viscosity, on the mode-coupling equations, following the theory of Oxtoby and Gelbart [17]. In those analyses the individual micelles were supposed to be a nearly monodispersed spherical structure, independent of temperature at least close to the critical point, i.e., in a domain corresponding to  $\epsilon \leq 10^{-2}$ . Here  $\epsilon$  is the reduced difference between the critical temperature  $T_c$  and the actual one  $T$ :  $\epsilon = |T - T_c|/T_c$ . Typically, the critical amphiphile weight concentration is of the order of a few percent and the first micelles formed in such dilute solutions are very likely spheroidal in shape [18]. However, one can expect that the micelles are rather polydispersed. The effect of polydispersity on the coexistence curve has been investigated extensively for the case of macromolecular solutions. As shown by Blankshtein *et al.* [19], a wide distribution in macromolecular sizes leads to a flat and asymmetric coexistence curve, an effect experimentally observed. A more recent explanation of the flatness and the skewness of the coexistence curve involves the intermicellar attractive potential, and these features appear to be a natural consequence of the interparticle attraction when using, for instance, Baxter’s potential. As a consequence of the flatness of the coexistence curve, the critical point is practically difficult to locate with a high precision.

The case of  $C_{12}E_5$  + water mixtures is much similar to

that described above, and the measured coexistence curve is extremely flat [10]. Close to the lower consolute point of mixing, the exponent  $\beta$ , which characterizes the temperature dependence of the order parameter  $C^+ - C^-$ , is apparently equal to 0.25 and so is much smaller than the expected 3D Ising value 0.33. Here,  $C^+$  and  $C^-$  denote the compositions of the concentrated and dilute phases at the two-phase equilibrium state. Our previous data sets obtained for this binary system indicated a somewhat puzzling behavior. For example, we experimentally observed a leveling-off in both  $\chi_T$  and  $\xi$  as a function of  $\epsilon$  in a region close to  $T_c$ . Besides, nearly mean-field values of  $\gamma \simeq 1.04$  and  $\nu \simeq 0.51$  were estimated in a wide range of temperature far from  $T_c$ , where  $\gamma$  and  $\nu$  characterize the temperature divergence of  $\chi_T$  and of  $\xi$ . Furthermore, the analysis of dynamical light-scattering measurements in terms of Kawasaki's mode-coupling theory [20] involved a considerably large contribution of the dynamical background term  $\Gamma_B$ . Its magnitude was typically more than 50% of the total relaxation rate  $\Gamma$  of the order-parameter fluctuations in the hydrodynamic regime and about 30% even in the critical regime. Some approximate equations have been proposed by Burstyn *et al.* [21] and by Rouch *et al.* [16] to account for the dynamical background term, assuming a cutoff parameter  $q_c$  linked to the inverse of the diameter of the micelle, on the basis of Oxtoby and Gelbart [17] predictions. These background calculations are, however, approximate and, as far as we know, no fully satisfactory model exists in the frame of generalized hydrodynamics theories for a mixture creating self-association in solution.

In recent years, the experimental results obtained for a ternary Aerosol OT (AOT)+water+decane microemulsion system and some of the nonionic amphiphile+water binary systems have been interpreted in terms of a modified version of the dynamical droplet model recently proposed by some of us [22]. Satisfactory results have been obtained when comparing our experimental data with the model [23]. In this model, proposed by Sorensen *et al.* [24] and Martin and co-workers [25] and modified using Coniglio and Klein results [26], it is assumed that the critical mixture is made of dilute polydispersed dynamical fractal clusters having a fractal dimension  $d_f$  and a polydispersity index  $\tau$ . Indeed from percolation theory, Coniglio and Klein [26] were able to reproduce the critical Ising-like behavior by putting  $d_f = d - \beta/\nu$  and  $d = d_f(\tau - 1)$ , leading to  $d_f \simeq 2.49$  and  $\tau \simeq 2.21$  [27], when  $\beta$  and  $\nu$  are assigned to the universal values relevant for a three-dimensional Ising system. In the above relations  $d = 3$  is the dimensionality of space. These values of  $d_f$  and  $\tau$  are very close to those relative to percolation. The analogy between the physical clusters and critical fluctuations has been recently investigated by Guenoun, Perrot, and Beysens [28] and Beysens, Guenoun, and Perrot [29] from direct visual observations of the order-parameter fluctuations near a critical point. They established experimentally the self-similarity of the physical clusters and obtained a fractal exponent  $d_f \sim 2.8$ , a value consistent with the theoretical estimate when the experimental errors are taken into account.

In this paper we report an extensive set of experimental data on the critical binary mixture  $C_{12}E_5$ +water. These data and those previously reported are first analyzed in terms of the generalized hydrodynamic theory of critical phenomena. Even by using nonuniversal values of the critical indices, some experimental results cannot be explained by the theory. We also used an extended version of the dynamical droplet model, in which the finite size of the monomer is taken explicitly into account. In this model, the critical clusters are treated like polydispersed fractal percolating aggregates having a fractal dimension  $d_f$  and a polydispersity index  $\tau$  which can be expressed in terms of the usual critical indices  $\gamma$ ,  $\nu$ , and  $\beta$ . A quantitative description of our full set of static and dynamic light-scattering data can be achieved by using universal 3D Ising values for the critical indices and realistic values for the short-range correlation length and the radius of the micelles.

## II. EXPERIMENT

Our apparatus and experimental procedures are similar to those described earlier [7,30]. Here, we give only the essential details. Pentaethylene glycol *n*-dodecylether ( $C_{12}E_5$ ) synthesized and purified by Nikko Chemical Co., Ltd. and water of liquid chromatographic quality (Wako Pure Chem. Ind., Ltd.) were used without further purification. Water was degassed just before preparation of the samples. The 6 mm diameter cylindrical glass cells were filled by solutions of different concentrations in a dry box containing dry nitrogen and then flame sealed under a mild vacuum. In order to deduce the critical weight concentration in amphiphile, the compositions of the two coexisting phases at the equilibrium state were measured along the coexistence curve [10]. The critical composition is  $C_c = (12.0 \pm 0.1)$  mg/g. Throughout this work we will use  $\epsilon$  as the reduced temperature difference between the temperature at which the demixing has been recorded for the concentration  $C = 12.0$  mg/g and the actual one. To reduce stray light effects, the scattering cell was immersed in a silicon oil bath ensuring a very good refractive index matching.

The distribution of scattered intensity was measured as a function of the scattering angle  $\theta$  in the reduced temperature range  $2.301 \times 10^{-5} \leq \epsilon \leq 2.132 \times 10^{-2}$  over the angular range of  $20^\circ \leq \theta \leq 135^\circ$  in steps of  $5^\circ$ . The corresponding wave vector  $q$  is given by  $q = 2q_0 \sin(\theta/2)$ , where  $q_0 = 1.325 \times 10^5 \text{ cm}^{-1}$  is the incident-light wave number, and is in the range  $4.602 \times 10^4 \leq q \leq 2.448 \times 10^5 \text{ cm}^{-1}$ . For each temperature, we carried out five experimental runs, whose standard deviations ranged typically from a few percent to 1%.

The long-term stability of samples containing surfactants at temperatures well above room temperature has been questioned and a chemical decay of the sample could be a severe limitation for an accurate study of the critical dynamics [31]. Close to the critical point phase-separation metastability effects can also affect the critical dynamics. To test possible nonequilibrium states and chemical decays of the samples close to the critical temperature, we measured the scattered light intensity at

four different angles, as a function of time for long periods, up to 5 days, for four fixed temperatures, respectively,  $\epsilon \approx 2.949 \times 10^{-5}$ ,  $\epsilon \approx 4.588 \times 10^{-5}$ ,  $\epsilon \approx 7.210 \times 10^{-5}$ , and  $\epsilon \approx 1.016 \times 10^{-4}$ . In addition, we measured the scattered light intensity over the entire angular range, from  $\theta = 20^\circ$  to  $135^\circ$  at a fixed temperature  $\epsilon \approx 9.832 \times 10^{-5}$ . In Fig. 1 we depict the typical behavior of the scattered intensity as a function of time for  $\epsilon \approx 7.210 \times 10^{-5}$ . For the full set of temperatures and angles we studied, the intensity has the same behavior as the one shown on Fig. 1, i.e., it remains constant, independent of time, over a period up to 100 h. This shows that the measurements were performed in a stationary state and that the chemical stability of the samples was ensured at least for this period of time.

Usually, the scattered light intensity  $I(q)$  is analyzed in terms of the Ornstein-Zernike (OZ) theory

$$I(q) = I_0 \frac{\chi_T}{1 + q^2 \xi^2},$$

where  $I_0$  is almost independent of temperature close to  $T_c$ . If the OZ relation is obeyed, a plot of  $[I(q)]^{-1}$  against  $q^2$  should be a straight line. In complex fluids this is not always the case, since static backgrounds can play a role. Therefore we have analyzed our  $q$ -dependent intensity data by using the following scaling static correlation function:

$$g(q\xi)^{-1} = 1 + \Sigma_2 q^2 \xi^2 - \Sigma_4 q^4 \xi^4, \quad (1)$$

where  $\Sigma_2$  and  $\Sigma_4$  are constant, set respectively to unity and zero in the OZ theory [32]. In simple fluids, a nonzero value in  $\Sigma_4$  is usually attributed to a small deviation from the OZ theory, which can be accounted for by the introduction of a small positive critical exponent  $\eta \approx 0.03$ , as suggested by Fisher [33]. Critical micellar systems are sometimes strong scatterers and attenuation of the incoming laser beam and of the scattered beam inside of the sample is to be accounted for by turbidity

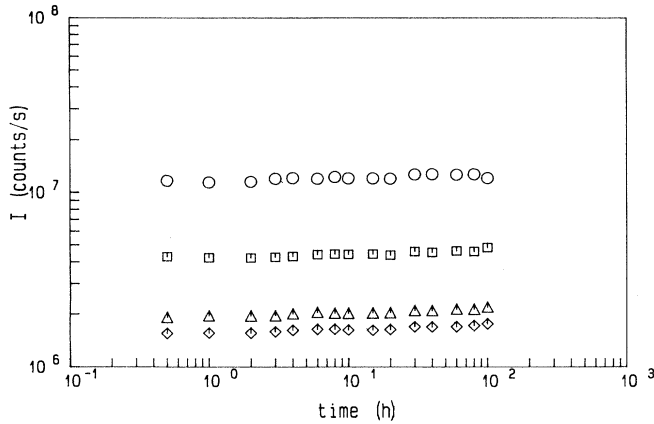


FIG. 1. The scattered light intensity as a function of time for the fixed reduced temperature  $\epsilon \approx 7.21 \times 10^{-5}$  at four scattering angles:  $\theta = 40^\circ$  (diamonds),  $\theta = 60^\circ$  (triangles),  $\theta = 90^\circ$  (squares),  $\theta = 120^\circ$  (circles).

effects. The total scattered intensity  $\Theta$  measured for the  $C_{12}E_5$  + water mixture was fitted to a polynomial function

$$\ln \Theta = \sum_{i=0}^6 a_i (\ln \epsilon)^{i-1}, \quad (2)$$

yielding  $a_0 = -15.639\,655\,8$ ,  $a_1 = -6.504\,731\,1$ ,  $a_2 = -1.387\,321$ ,  $a_3 = -1.581\,22 \times 10^{-1}$ ,  $a_4 = -9.029\,173\,7 \times 10^{-3}$ , and  $a_5 = -2.014\,358\,7 \times 10^{-4}$ , whose values were used for attenuation corrections. The magnitude of those corrections was 15% at  $\epsilon \approx 2.3 \times 10^{-5}$  and 8% at  $\epsilon \approx 5.6 \times 10^{-4}$ . It is known that in light-scattering measurements very close to the critical point, multiple scattering also causes apparent deviations from Ornstein-Zernike behavior [34]. A rough evaluation of the multiple-scattering contribution shows that it is at most 6% and less than 0.1% for the same values of  $\epsilon$ . Since our main interest in this work is directed toward general aspects of critical properties not too close to  $T_c$  (mainly in the hydrodynamic regime), we will not perform multiple-scattering corrections in the present analysis. Let us also check here the long-term stability of the sample. The extrapolated zero angle scattered intensity  $I(0) = \lim_{q \rightarrow 0} I(q)$  and the correlation length  $\xi$  are shown as a function of time for a fixed temperature  $\epsilon \approx 9.832 \times 10^{-5}$  in Fig. 2. It can be seen that the values of both  $[I(0)]^{-1}$  and  $\xi$  are constant well independent of time over a very long period confirming the results given above.

From dynamical light-scattering experiments, we have measured the time-dependent order-parameter correlation function at four different angles, respectively,  $\theta = 40^\circ$ ,  $60^\circ$ ,  $90^\circ$ , and  $120^\circ$  in the temperature range of  $6.556 \times 10^{-6} \leq \epsilon \leq 1.659 \times 10^{-3}$ . In order to minimize the multiple-scattering contribution [35], we used a 4 mm diameter cylindrical cell. The phototube signal was analyzed by a 48-channel Malvern K7023 single-clipped correlator. The measured time-dependent intensity correlation function shows systematic deviations from the single-exponential decay law observed for simple fluids or molecular binary mixtures. Hence, we analyzed our experimental data with a quadratic polynomial given

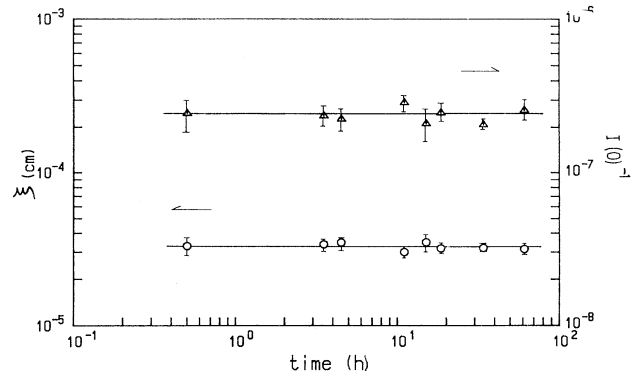


FIG. 2. The inverse zero-scattered light intensity  $[I(0)]^{-1}$  (triangles) and the long-range correlation length  $\xi$  (circles) as a function of time at a fixed value of  $\epsilon \approx 9.83 \times 10^{-5}$ .

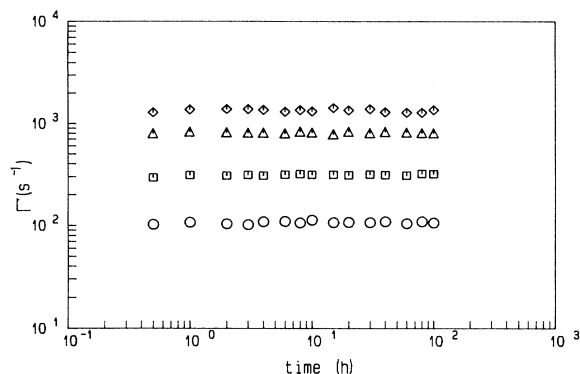


FIG. 3. The relaxation rate  $\Gamma$  as a function of time for a fixed reduced temperature  $\epsilon \approx 7.21 \times 10^{-5}$  at four angles of scattering:  $\theta = 40^\circ$  (circles),  $\theta = 60^\circ$  (squares),  $\theta = 90^\circ$  (triangles),  $\theta = 120^\circ$  (diamonds).

by

$$\ln G(t) = K_0 - K_1 t + \frac{1}{2} K_2 t^2, \quad (3)$$

where  $K_n$ , the  $n$ th cumulant, can be deduced by fitting the experimental decay of the correlation function. The normalized second moment  $k = K_2/K_1^2$  denotes the magnitude of the deviations from the single-exponential decay. In Fig. 3 we show the decay rate (first cumulant) measured at a fixed temperature of  $\epsilon \approx 7.210 \times 10^{-5}$  as a function of time. Also in the dynamic case our data show that the decay-rate values at four scattering angles are independent of time.

To measure the viscosity of the critical mixture we used a rotational viscometer with concentric cylinders separated by a narrow gap ( $1.00 \pm 0.04$  mm), in which the inner cylinder was rotating [30,36–38]. A provision was made enabling us to observe simultaneously the light scattered by the mixture filled in the gap under dry nitrogen. We determined the critical temperature by observing the appearance of a spinodal ring around the directly transmitted central spot on a screen for each experimental run. We operated the instrument at low shear rates in the range of  $0.4 \leq S \leq 0.5$  s $^{-1}$ . The viscometer was calibrated against water and the viscosity was calculated from the angular speed of the inner cylinder for a fixed value of the torque exerted on it. Three experimental runs were carried out for the critical mixture in the temperature ranges, respectively, of  $7.368 \times 10^{-3} \leq \epsilon \leq 2.675 \times 10^{-2}$ ,  $3.275 \times 10^{-6} \leq \epsilon \leq 7.335 \times 10^{-3}$ , and  $6.547 \times 10^{-6} \leq \epsilon \leq 3.274 \times 10^{-3}$ .

We will discuss in the next section the critical behavior of mixtures of  $C_{12}E_5$  + water, including our earlier experimental data, some of which have not been reported in detail. Throughout this work we will make no distinction between our earlier experimental data and the data measured in the present work.

### III. EXPERIMENTAL RESULTS

#### A. Intensity data

The scattered intensity has been measured at a fixed angle  $\theta = 90^\circ$  corresponding to  $q = 1.874 \times 10^5$  cm $^{-1}$ , over

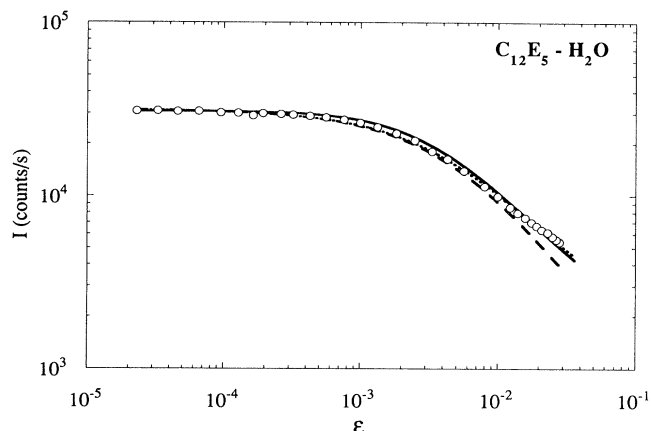


FIG. 4. The scattered intensity as a function of the reduced temperature. The circles are experimental data, the dashed line is the best fit of the data to the OZ theory with free values of the indices, the dotted line is the best fit of the data to the OZ theory including a static background with universal values of the indices. The full line is the best fit of the data to Eq. (5).

the temperature range of  $2.301 \times 10^{-5} \leq \epsilon \leq 2.311 \times 10^{-2}$  with typical errors comprised between 0.3% and 1.4%. It is shown as a function of  $\epsilon$  in Fig. 4. Here we start out by recalling our previous results [9] obtained from the angular distribution of scattered light intensity. In this previous analysis we estimated the exponent values of  $\gamma \approx 1.04$  and  $\nu \approx 0.51$  in a temperature range of  $4.7 \times 10^{-4} \leq \epsilon \leq 1.8 \times 10^{-2}$ . To compare our previous results with the present ones, we have fitted our data depicted in Fig. 4 and spanning the temperature range of  $5.6 \times 10^{-4} \leq \epsilon \leq 2.3 \times 10^{-2}$  to the OZ function with  $\Sigma_2 = 1$  and  $\Sigma_4 = 0$  in Eq. (1), assuming universal values of  $\gamma = 1.239$  and  $\nu = 0.630$ . We also included phenomenologically a constant static background term  $I_B$ . This procedure yields a large systematic error with a maximum deviation of about  $\pm 40\%$ . We also tried to fit the same data set by considering a temperature-dependent background  $I_B(\epsilon)$ . Even in this case, a significantly periodic error with a maximum deviation of  $\pm 10\%$  was observed. With the values of  $\gamma = 1.035$ ,  $\nu = 0.514$ , and  $\xi_0 \approx 3.27$  nm estimated previously [9], the best fit of the intensity data to the OZ function was obtained in the corresponding range of  $\epsilon$ . In this case a temperature-dependent background  $I_B(\epsilon) = a\epsilon^2 + b\epsilon + c$  was assumed. So the best fit to the data using the OZ formula leads to a short-range correlation length  $\xi_0 \approx 3.27$  nm much larger than that usually found for micellar aggregates,  $\xi_0 \approx 1$  nm and to apparently nonuniversal values of the indices  $\gamma$  and  $\nu$ . These results are very similar to those we reported previously. Besides, we also reported that, sufficiently close to  $T_c$ , both quantities  $[I(0)]^{-1}$  and  $\xi$  level off, in contrast to the expected power-law divergences. In Fig. 5 we plot  $\xi$  and  $[I(0)]^{-1}$  as a function of  $\epsilon$ . The solid lines correspond to the power-law behaviors of  $\xi \propto \epsilon^{-\nu}$  with  $\nu \approx 0.51$  and of  $[I(0)]^{-1} \propto \epsilon^\gamma$  with  $\gamma \approx 1.04$ . In the region  $\epsilon \leq 4 \times 10^{-4}$ , both quantities tend to be constant, suggesting nondivergent behaviors. In order to show

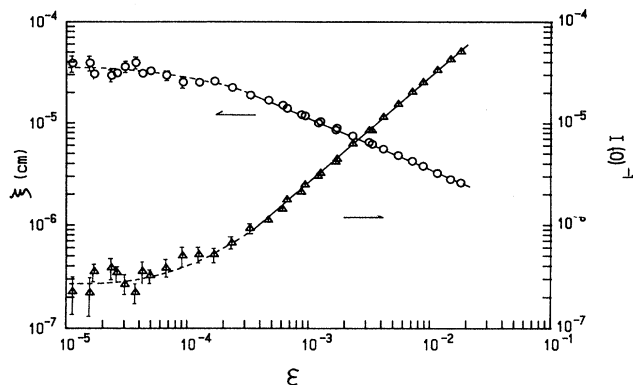


FIG. 5. The inverse zero-scattered intensity  $[I(0)]^{-1}$  and the correlation length  $\xi$  as a function of  $\epsilon$ . The solid lines denote power laws with slopes of  $\gamma \approx 1.04$  and  $\nu \approx 0.51$ , respectively.

more vividly a clear deviation from the linear behavior representing a power law in the double logarithmic plot, the quantities  $\Delta I(0) = [I(0)]^{\text{calc}} - I(0)$  and  $\Delta \xi = \xi^{\text{calc}} - \xi$  are plotted as a function of  $\epsilon$  in Fig. 6. Here  $[I(0)]^{\text{calc}}$  and  $\xi^{\text{calc}}$  denote the extrapolated values within the region  $\epsilon \leq 4 \times 10^{-4}$  using the power law as represented by the solid line of Fig. 6. Thus the measured values of  $\xi$  and  $I(0)$  and are well represented by  $\xi = \xi^{\text{calc}} - \Delta \xi$  with  $\Delta \xi = (2.4 \pm 1.2) \times 10^{-9} \epsilon^{-0.92 \pm 0.05}$  cm and by  $I(0) = [I(0)]^{\text{calc}} - \Delta I(0)$  with  $\Delta I(0) = (9.6 \pm 3.5) \epsilon^{-1.34 \pm 0.04}$ . It is noted that considerably large discrepancies can be observed, for example, a factor of about 2.5 in  $\xi$  at  $\epsilon \sim 10^{-5}$ .

It has to be remarked that for a mixture at the critical composition, the compressibility and the long-range correlation length diverge at the critical point, while they remain finite at off-critical phase-separation points. Consequently, one might expect that our light-scattering measurements performed on the sample at composition 12 mg/g were carried out for a noncritical mixture, i.e., along an off-critical isochore. To explore in more detail

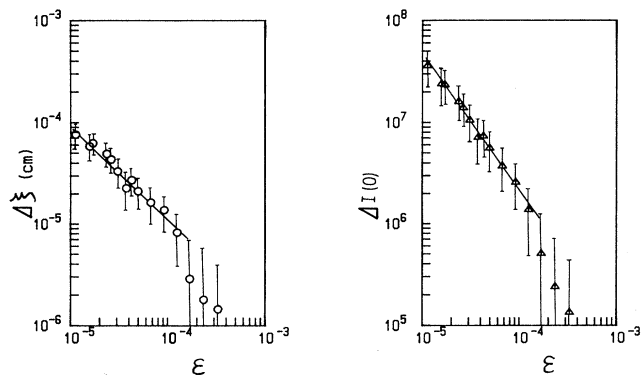


FIG. 6. The quantities  $\Delta I(0) = [I(0)]^{\text{calc}} - I(0)$  and  $\Delta \xi = \xi^{\text{calc}} - \xi$  as a function of  $\epsilon$ , where the solid lines represent the slopes of  $-1.34$  and  $-0.92$ , respectively. The calculated values in  $[I(0)]^{\text{calc}}$  and  $\xi^{\text{calc}}$  are given by the power law represented by the solid lines appearing in Fig. 5.

the behaviors of  $[I(0)]^{-1}$  and  $\xi$  we have performed light-scattering measurements along various isochores covering the concentration range from  $C \approx 5.81$  to  $C \approx 15.4$  mg/g. The temperatures  $T_p$  corresponding to phase separation were determined in the entire concentration range investigated here by the onset of the so-called spinodal ring of the forward scattering of light [36]. Again, and as expected, since we are now not studying a critical sample, saturation effects in  $[I(0)]^{-1}$  and in  $\xi$  are observed in the double logarithmic plots vs the reduced temperature difference  $\epsilon_p$  defined by  $\epsilon_p = (T_p - T)/T_c$ . To reproduce the power-law behavior for the osmotic compressibility and the long-range correlation length deduced from light-scattering experiments, we assume for each composition a divergence of the relevant quantity at a temperature  $T_d$  inside the two-phase region of the phase diagram of the mixture  $C_{12}E_5 + \text{water}$ , which should correspond to the spinodal line [37]. We expect that it would be possible to fit the data to a power law as long as the pseudospinodal concept can be assumed for any isoconcentration line. At the critical composition, the pseudospinodal temperature  $T_{sp}$  should be identical to  $T_p \equiv T_c$ , namely,  $T_{sp} - T_c = 0$ . Strictly speaking, a power-law divergence along an off-critical isochore may not be valid as shown by model equations of state [39], although relevant parameters like the compressibility diverge along the spinodal curve. However, for samples having compositions not too far from the critical one, numerical results deduced, for instance, from linear or cubic equations of state, are in agreement with the pseudospinodal concept. In the present analysis we treated  $\Delta \epsilon = (T_d - T_p)/T_c$ ,  $\xi_0$ , and  $\nu$  as free parameters to fit the experimental data of the long-range correlation length  $\xi$  to a simple power law

$$\xi = \xi_0 (\epsilon + \Delta \epsilon)^{-\nu} . \quad (4)$$

Our  $T_d$  should be identical to  $T_{sp}$  if the pseudospinodal concept is valid in the present case. The results deduced from Eq. (4) are summarized in Table I. The values of  $\xi_0$  and  $\nu$  averaged over the concentration range of  $8.7_4 \leq C \leq 15.3_6$  mg/g were  $\xi_0 = 2.1 \pm 0.3$  nm and  $\nu = 0.61 \pm 0.03$ . We excluded the values obtained at the concentration  $C = 5.8_1$  mg/g since, as discussed above, this composition is too different from the critical one. In the case depicted in Fig. 5 for the mixture having the concentration  $C = 12.0$  mg/g, we obtained  $\xi_0 = (2.0 \pm 0.6)$  nm,  $\nu = 0.60 \pm 0.05$ , and  $\Delta \epsilon = (1.6_9 \pm 0.4_0) \times 10^{-4}$  by fitting the data to Eq. (4). The fit of  $[I(0)]^{-1}$  to a similar power law as in Eq. (4) also leads to  $\gamma = 1.22 \pm 0.09$  and  $\Delta \epsilon = (1.7_8 \pm 0.4_0) \times 10^{-4}$ . The estimated values of  $\Delta \epsilon$  deduced from both  $[I(0)]^{-1}$  and  $\xi$  are very similar within experimental errors, and the indices  $\gamma$  and  $\nu$  have values very close to the universal ones. Besides, a universal value of  $\beta = 0.32_1 \pm 0.02_2$  can be obtained by fitting the coexistence curve of  $C_{12}E_5 + \text{water}$  in the temperature range of  $9.835 \times 10^{-6} \leq \epsilon \leq 1.665 \times 10^{-3}$  if we take the value of  $\Delta \epsilon \sim 10^{-5}$ . These results clearly indicate that the Ising values of the critical indices can be obtained when a nonzero, although very small, value of  $\Delta \epsilon$  is considered, while  $\Delta \epsilon$  does not go to zero in the en-

TABLE I. Values of  $\Delta\epsilon$ ,  $\xi_0$ , and  $\nu$  at various concentrations  $C$ .

$C$ (mg/g)	$\Delta\epsilon$	$\xi_0$ (nm)	$\nu$
5.81	$(1.2\pm 0.9)\times 10^{-3}$	$3.0\pm 2.2$	$0.54\pm 0.16$
8.74	$(4.2\pm 0.9)\times 10^{-4}$	$2.1\pm 0.4$	$0.61\pm 0.03$
10.13	$(6.3\pm 1.0)\times 10^{-5}$	$2.8\pm 0.3$	$0.57\pm 0.02$
11.19	$(1.8\pm 0.3)\times 10^{-4}$	$1.6\pm 0.2$	$0.65\pm 0.02$
13.37	$(2.1\pm 0.3)\times 10^{-4}$	$1.9\pm 0.2$	$0.60\pm 0.02$
15.36	$(2.2\pm 0.3)\times 10^{-4}$	$1.7\pm 0.2$	$0.60\pm 0.02$

tire concentration range investigated in this work. A similar result has been reported by Seto *et al.* for a microemulsion system [40].

As mentioned earlier, one observes a tendency to an upward curvature of the plot of the intensity as a function of  $\epsilon$  at higher distances in temperature from the critical point as shown in Fig. 4. This effect, also observed for microemulsion systems, is only sizable when the critical solution is made of supramolecular aggregates. In order to account for these features, we use the structure factor associated with the dynamical droplet model. It has been recently derived for fractal polydispersed aggregates by Tartaglia and co-workers [22] from the Chen and Teixeira calculation [41], and includes Fisher's correction. The scattered light intensity  $I(q)$  is given by

$$I(q) = I_0 \left[ \frac{x}{x_1} \right]^{d_f} (1+x^2)^{d_f(\tau-3)/2} \times \frac{\Gamma(3-\tau, (x_1/x)^{d_f} (1+x^2)^{d_f/2})}{\Gamma(2-\tau, (x_1/x)^{d_f})}, \quad (5)$$

where  $I_0$  is a term depending upon the geometry of the experiment and almost independent of temperature close to  $T_c$ ,  $x = q\xi$  the scaling variable,  $\Gamma(u, v)$  the incomplete Euler gamma function, and  $x_1 = qR_1$  is the reduced size of the individual micelle. In this equation a finite-size contribution associated with micelles themselves has been explicitly taken into account via  $x_1$ . In the frame of earlier approaches on light scattering from critical systems this contribution sometimes has been treated as the non-trivial background term. Thus, from the fits of our intensity data to Eq. (5) we would gain insight into the finite-size contribution associated with self-assembling microstructures. This has been done for our intensity data depicted in Fig. 4 which were fitted to Eq. (5). The best fit to the data leads to the fractal dimension  $d_f = 2.50 \pm 0.10$  and to the polydispersity index  $\tau = 2.35 \pm 0.10$ . These values are compatible with the theoretical estimates to within experimental errors and lead to values of the critical indices that are very close to the universal ones. The two other fitted parameters involved in Eq. (5) are the short-range correlation length  $\xi_0$  and the radius  $R_1$  associated with an effective micellar size. The estimated values of these parameters for the mixture  $C_{12}E_5 + \text{water}$  are  $\xi_0 = 1.4 \pm 0.1$  nm and  $R_1 = 2.8 \pm 0.2$  nm, respectively. The value of  $\xi_0 \approx 1.4$  nm inferred from the modified version of the droplet model is almost consistent with the one  $\xi_0 = 1.68 \pm 0.05$  nm obtained from a fit of the data

shown in Fig. 5 to a power law [Eq. (4)] by setting  $\gamma = 1.239$  and  $\nu = 0.630$ . The present result is shown in Fig. 4 in comparison with the fit to the OZ function, in which the solid curve represents the calculated one of Eq. (5) with  $d_f = 2.50$ ,  $\tau = 2.35$ ,  $\xi_0 = 1.4$  nm, and  $R_1 = 2.8$  nm. In the figure the broken and dotted curves are the fits to the OZ function without a background term and a constant background  $I_B$ , respectively. Besides, Eq. (5) gives  $[I(0)]^{-1} = \lim_{q \rightarrow 0} [I(q)]^{-1}$  in the form

$$[I(0)]^{-1} = I_0^{-1} \left[ \frac{R_1}{\xi} \right]^{d_f} \frac{\Gamma(2-\tau, (R_1/\xi)^{d_f})}{\Gamma(3-\tau, (R_1/\xi)^{d_f})}. \quad (6)$$

In Fig. 7 we show the calculated curve of Eq. (6) by setting the parameter values of  $d_f = 2.50$ ,  $\tau = 2.35$ ,  $\gamma = 1.239$ ,  $\nu = 0.630$ ,  $\xi_0 = 1.4$  nm, and  $R_1 = 2.8$  nm. In the figure the experimental data are plotted against a modified value  $\epsilon^* = \epsilon + \Delta\epsilon$  with  $\Delta\epsilon = 1.74 \times 10^{-4}$ . It should be noted that a fairly good agreement can be observed between the experimental data and the calculated curve predicted by Eq. (6), the indices being assigned to the 3D Ising values, by putting  $\Delta\epsilon \sim 10^{-4}$ .

### B. Dynamical data

The decay rate of the order parameter measured for solutions of  $C_{12}E_5$  in water has been analyzed using Eq. (3). The observed deviations of the time-dependent correlation function from a single-exponential decay were

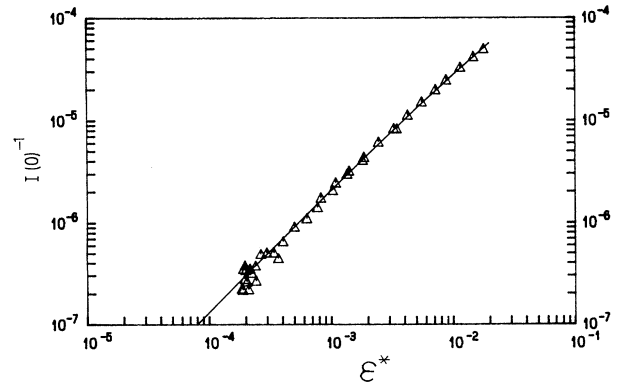


FIG. 7. The zero-scattered intensities as a function of the modified reduced temperature  $\epsilon^* = \epsilon + \Delta\epsilon$ , where the solid line represents the calculated curve of Eq. (6) setting  $d_f = 2.50$ ,  $\tau = 2.35$ ,  $\gamma = 1.239$ ,  $\nu = 0.630$ ,  $\xi_0 = 1.4$  nm, and  $R_1 = 2.8$  nm.

significantly large. For example, typical values of the normalized second cumulant  $k$  were  $k=0.32\pm 0.16$  at  $\epsilon=3.852\times 10^{-3}$ . The measured relaxation rate of the scattered field (or intensity) correlation function not only reflects the temporal decay of the order-parameter fluctuations depending on temperature and wave vector, but may be influenced also by a possible existence of dust particles in the mixture, and by stray light scattered from the glass walls of the sample cell. In our case, the contributions to the decay rate induced from stray light and from dust particles were at most a few percent, over the entire angular ranges [42]. The crude estimated value of  $k$  was  $k=0.03\pm 0.02$  in the range of  $6\times 10^{-2}\leq \Gamma t\leq 2$  at  $\epsilon\approx 0$ . On the other hand, we obtained  $k=0.22\pm 0.06$  at  $\epsilon\approx 3.84\times 10^{-2}$ , i.e., at large distance from  $T_c$ . Roughly speaking, the deviation from the single-exponential law is little as  $\epsilon$  goes to small values, while the  $k$  values remain relatively large at higher distances from  $T_c$ . To physically explain the nonexponential behavior of the scattered field correlation function, we exclude contributions due to a frequency-dependent critical viscosity as predicted by Ferrell and co-workers [43], which would lead to too small effects [44]. More likely, we conjecture that the observed deviations from a single-exponential decay should be attributed to significant contributions due to the finite-size effect associated with molecular aggregates of  $C_{12}E_5$  in water. This effect has been recently experimentally observed for a critical microemulsion system by using a logarithmic correlator [22].

Analyses of the decay rate (first cumulant) of the time-dependent correlation function associated with the order-parameter fluctuations are usually made in the frame of mode-coupling theories of critical phenomena including dynamical background contributions. In these theories, the decay rate  $\Gamma$  measured near the critical point is given as the sum of a critical part  $\Gamma_c$  and a background part  $\Gamma_B$ , i.e.,  $\Gamma=\Gamma_c+\Gamma_B$ . The critical part  $\Gamma_c$  can be represented by

$$\Gamma_c = \Gamma - \Gamma_B = Rq^3 \frac{k_B T}{6\pi\eta(T)} \Omega(x), \quad (7)$$

where  $R\approx 1.03$  is the universal amplitude ratio and  $\Omega(x)$  the dynamical universal function. The viscosity  $\eta(T)$  is given by

$$\eta(T) = \eta_B (Q_0 \xi)^{x_\eta} = \eta_B (Q_0 \xi_0)^{x_\eta} \epsilon^{-\phi}, \quad (8)$$

in which  $\eta_B$  is the nonsingular part of the viscosity,  $Q_0$  a cutoff parameter, and  $x_\eta = \phi/\nu$  the critical viscosity exponent. The universal value of  $\phi\approx 0.04$  has been found for many critical mixtures [45]. In general, a micellar system has been regarded as shear-sensitive fluid, whose viscosity tends to exhibit non-Newtonian behavior near the critical consolute point. This implies that, very close to  $T_c$ , shear flow in the viscometer tends to affect viscosity data, giving rise to a leveling off. To minimize these effects, a low-shear rotational viscometer was used in this work. The universal value of  $\phi\approx 0.04$  has been obtained using the low-shear viscometer employed for the critical micellar systems  $C_6E_3$  + water and  $C_{10}E_4$  + water studied previously [46]. Since the magnitude of the shear effect

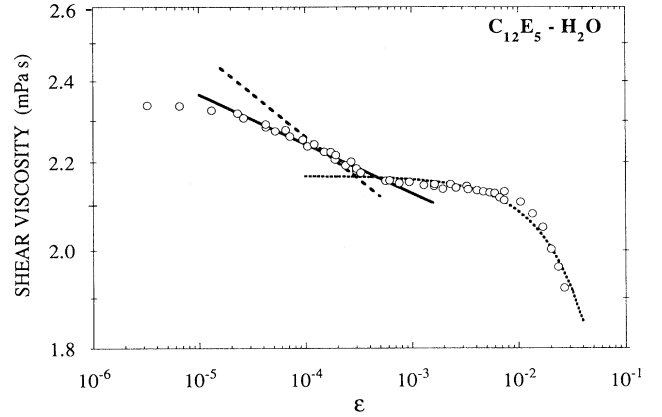


FIG. 8. The shear viscosity as a function of the reduced temperature. The circles are experimental data, the full line is the best fit of the data, taken close to  $T_c$ , to a power law, the dash-dot line is a power law with a slope of  $-0.04$ , whereas the solid line is the best fit of the data, taken far from  $T_c$ , to an Arrhenius law.

depends on the product of the shear rate and the lifetime of the fluctuations [47], this implies that shear effects not only depend on the reduced temperature but also on the mixtures themselves. In Fig. 8 we show our viscosity data taken for  $C_{12}E_5$  + water in a low range of shearing. Since the measured viscosity is approximately insensitive to the temperature variation in the range  $\epsilon\sim 2\times 10^{-3}$ , we used here the value of  $\eta_B\approx 2.15$  mPa s at  $\epsilon\approx 2.3\times 10^{-3}$  as the background viscosity in the critical region. The fit to the experimental data leads to the amplitude  $A=(Q_0\xi_0)^{x_\eta}=0.85\pm 0.02$  and  $\phi=0.023\pm 0.004$  in the temperature range  $2.6\times 10^{-5}\leq \epsilon\leq 3.3\times 10^{-4}$ , the data points showing the leveling off being discarded in the analysis. The value we estimated for the exponent  $\phi$  is lower than the universal one expected for a fluid system, i.e., 0.04. In turn, we analyzed all data points within the critical region ( $\epsilon\leq 3.3\times 10^{-4}$ ) by considering of a nonzero value of  $\Delta\epsilon$  and treating  $\phi$ , the amplitude ratio  $A$ , and  $\Delta\epsilon$  as free parameters. We then obtain  $\phi=0.033\pm 0.003$ ,  $A=1.68\pm 0.03$ , and  $\Delta\epsilon=(3.6\pm 0.8)\times 10^{-5}$ . Considering the difficulty of the experiments, a possible influence of the shear flow even at low shear rate, and the temperature range of fitting, the difference between the present value of  $\phi=0.033\pm 0.003$  and the universal one 0.04, is not very large, so that in turn we tried to fit our viscosity data by setting  $\phi=0.04$ . This yielded  $A\approx 1.6$  and  $\Delta\epsilon\approx 6\times 10^{-5}$ . Again, it is noted that the universal value in the viscosity exponent can be obtained by considering a small temperature shift  $\Delta\epsilon\sim 10^{-4}$ .

The recently proposed dynamical universal function  $\Omega(x)$  can be represented by

$$\Omega(x) = (1/x^3)K(x)[S(x)]^{x_\eta}, \quad (9)$$

where  $K(x)$ , Kawasaki's function, is given by

$$K(x) = \frac{3}{4} \left[ 1 + x^2 + \left( x^3 - \frac{1}{x} \right) \tan^{-1} x \right], \quad (10)$$

and  $S(x)$ , the correction to scaling, by  $S(x) = [1 + (b/a_0)^2 x^2]^{1/2}$ . The coefficient  $a_0$  is related to the universal amplitude ratio  $R$  by  $R = a_0^{\eta}$ . Analytical expressions of the background part  $\Gamma_B$  have been proposed both by Burstyn *et al.* [21] and by Oxtoby and Gelbart [17]. The Burstyn *et al.* formula reads

$$\Gamma_B = q^2 \frac{k_B T}{16\eta_B \xi} \frac{1 + q^2 \xi^2}{q_c \xi}, \quad (11)$$

where  $q_c$  is a Debye cutoff wave number. On the other hand, the one derived from Oxtoby and Gelbart is

$$\Gamma_B = RCq^2 \frac{k_B T}{8\pi\eta_B \xi} \frac{1 + q^2 \xi^2}{q_c \xi}, \quad (12)$$

where  $C$  is a numerical constant of the order of 0.9. Applying this formula to a microemulsion system, Rouch *et al.* [16] were able to show that the inverse of the Debye cutoff is of the order of the diameter of the microemulsion droplet. In the frame of the modified version of the dynamical droplet model, it can be shown [23] that the first cumulant (decay rate) is given by

$$\Gamma(x, x_1) = R \frac{k_B T}{16\eta(T)} q^3 \frac{\Gamma(3 - \tau, x_1^{d_f})}{\Gamma(3 - \tau - (1/d_f), x_1^{d_f})} \times \frac{\Gamma(3 - \tau - (1/d_f), u)}{\Gamma(3 - \tau, u)} \left[ 1 + \frac{1}{x^2} \right]^{1/2}, \quad (13)$$

where  $u = (x_1/x)^{d_f} (1 + x^2)^{d_f/2}$ . Equation (13) reduces exactly to the Perl and Ferrell mode-decoupling result [43] when the radius of the monomer  $R_1 \rightarrow 0$  and, in this case, it is numerically very close to Kawasaki's formula [20]. However, when the radius of the individual micelles, supposed to be spherical and monodispersed, is not very small compared to the correlation length, significant deviations are expected from generalized hydrodynamic models. In fact, numerical simulations [23] show that when  $R_1 \neq 0$  a leveling off of the linewidth is observed far from the critical point, in qualitative agreement with the experimental findings. So the dynamical background discussed above and connected to the finite-size effect of the monomers should be accounted for, at least partially, by the extended version of the dynamical droplet model.

The experimental values of the decay rates have been compared to the three models quoted above using different fitting procedures. First of all, data have been fitted to Kawasaki's equation including a background [Eq. (11) or (12)] with a fixed value of the amplitude  $R = 1.03$  as deduced from the mode-coupling theory and indices equal to their universal values, the Debye cutoff parameter  $q_c$  being free. Even a moderately good fit to the full set of data obtained at different scattering angles cannot be obtained with a single value of  $q_c$ . So this quantity appears to be strongly wave-vector-dependent, which is unrealistic. If a best fit is performed to data obtained at the lowest  $q$  value corresponding to a scattering

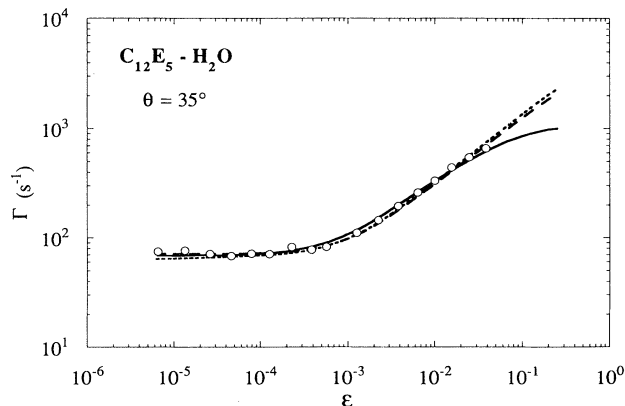


FIG. 9. Comparison of the theoretical models with the relaxation rate associated with the order-parameter fluctuations as a function of the reduced temperature for a value of the scattering angle of  $\theta = 35^\circ$ . The circles are experimental data, the full line is the best fit of the data to Eq. (13) (dynamical droplet model), the dotted line is the best fit of the data to Oxtoby and Gelbart [Eq. (12)], and the dashed line is the best fit of the data to Burstyn *et al.* [Eq. (11)].

angle of  $35^\circ$  and assuming that the indices are universal,  $R$  being a free parameter, the following values are obtained:  $\xi_0 = (1.40 \pm 0.05)$  nm,  $q_c = (1.0 \pm 0.2)$  nm $^{-1}$ , and  $R = 1.15 \pm 0.05$  using the equation of Burstyn [Eq. (11)], and  $\xi_0 = (1.40 \pm 0.05)$  nm,  $q_c = (1.0 \pm 0.2)$  nm $^{-1}$ , and  $R = 1.15 \pm 0.05$  using the equation of Oxtoby and Gelbart [Eq. (12)]. We can now use these numerical values of the parameters to calculate the linewidth for the other wave vectors. The results we got are depicted in Figs. 9–13. It can be seen that the Burstyn *et al.* [21] model significantly deviates from the experimental findings, even in the critical regime at the largest value of the wave vector. This is not the case when using the Oxtoby and Gelbart [17] model. However, this model does not accurately describe data taken far from the critical point.

On the other hand, fitting the data to the dynamical

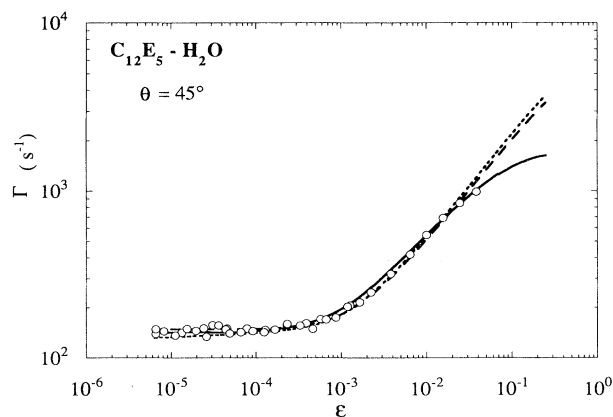


FIG. 10. The relaxation rates measured at the scattering angle  $\theta = 45^\circ$  as a function of  $\epsilon$ . The symbols are the same as those of Fig. 9.

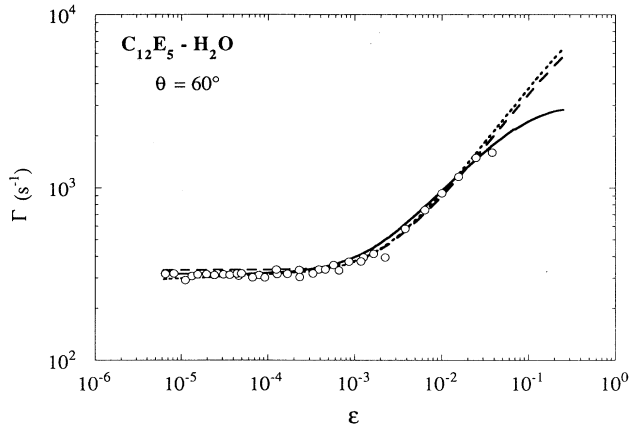


FIG. 11. The relaxation rates measured at the scattering angle  $\theta=60^\circ$ . The symbols are the same as those of Fig. 9.

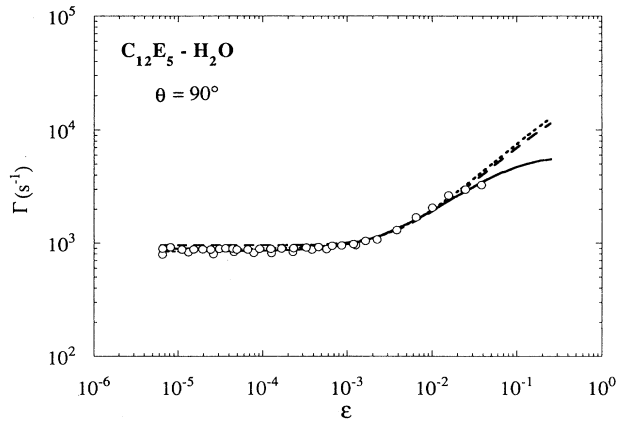


FIG. 12. The relaxation rates measured at the scattering angle  $\theta=90^\circ$ . The symbols are the same as those of Fig. 9.

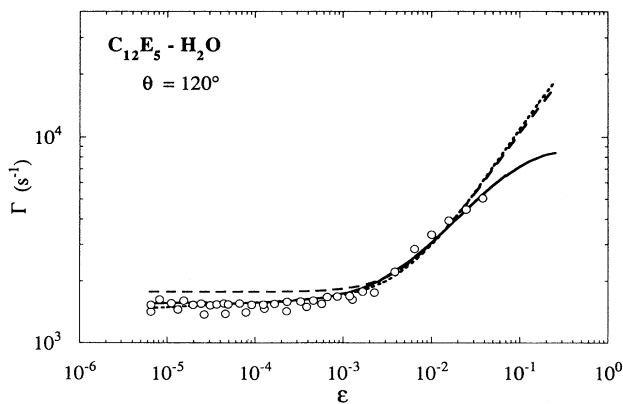


FIG. 13. The relaxation rates measured at the scattering angle  $\theta=120^\circ$ . The symbols are the same as those of Fig. 9.

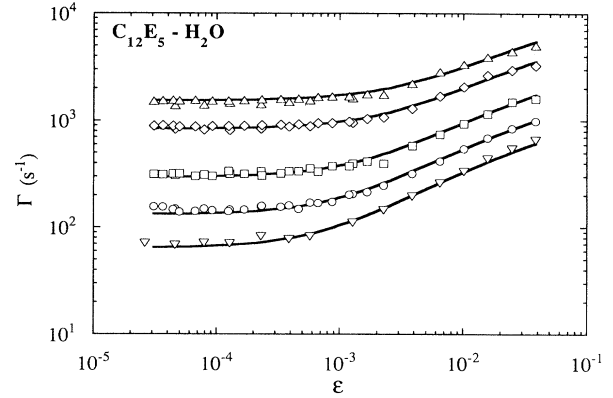


FIG. 14. Comparison of experimental relaxation rate of the order parameter with the calculated ones following the modified dynamical droplet model of Eq. (13). The symbols refer to measurements:  $\theta=35^\circ$  (inverted triangles),  $\theta=45^\circ$  (circles),  $\theta=60^\circ$  (squares),  $\theta=90^\circ$  (diamonds),  $\theta=120^\circ$  (triangles).

droplet model [Eq. (13)] with universal values of the indices leads to  $\xi_0=(1.4_0\pm 0.05)$  nm,  $R_1=(2.8\pm 0.2)$  nm, and  $R=1.00\pm 0.05$ . It can be seen in Fig. 14 that the calculated linewidths are in very good agreement with experiments not only in the critical regime but also in the hydrodynamic regime, even far from the critical point. Moreover, the values of the fitted coefficients  $\xi_0$  and  $R_1$  are in this latter case the same as those used to fit the intensity data and the coupling constant  $R$  is very close to its universal value 1.03.

#### IV. DISCUSSION

First, forcing our experimental data to fit the OZ theory and the mode-coupling formulas without including static and dynamical backgrounds leads to bad results and to nonuniversal values of the critical indices. Besides, the values inferred for  $\xi_0$  from the static and dynamical critical phenomena differ by a factor of the order of 2, showing the inconsistency of the procedure. On the other hand, a fairly good fit to the data can be obtained by using universal values for the indices owing to the introduction of large nonuniversal static and dynamical backgrounds. Considerable efforts have been devoted to describing the thermodynamic and transport properties of fluids in terms of a crossover from the singular behavior in the critical region to the regular behavior far away from the critical point [48]. But as far as we know, no model is currently available to treat the static and dynamical backgrounds or micellar solutions including a non-negligible finite-size effect due to self-association in solution. Therefore the contributions to the critical parts appear as *ad hoc* phenomenological background terms.

When using the modified version of the dynamical droplet model, a very good fit to the static and dynamical properties can be achieved without introducing any background. In this case however, the value we deduced for the polydispersity index  $\tau$  from intensity is slightly greater than the theoretical estimate. This can be ex-

plained by the experimental findings of di Meglio *et al.* [49], who observed a non-negligible amount of dimers close to the critical point of the same mixture, thereby increasing the apparent polydispersity of the sample. On the other hand, the universal value of  $\tau$  can be used to fit the relaxation rate of the order parameter since this quantity is less sensitive to polydispersion than intensity. Furthermore, the numerical value 2.8 nm we deduced for the radius of the monomer  $R_1$  is in good agreement with the experimental determination, namely 2.3 nm, given by di Meglio *et al.* [49]. It is also consistent with values close to 3.0 nm obtained on  $C_{12}E_8 + H_2O$  by different authors [14,50,51], the chain length of the  $C_{12}E_8$  surfactant molecule being slightly larger than that of  $C_{12}E_5$ .

We believe that the most accurate value for  $\xi_0$  is about 1.4 nm, since it is close to that given in Refs. [4,5] for the systems  $C_{12}E_6 + H_2O$  and  $C_{12}E_8 + H_2O$ , the nonionic surfactant molecules of these solutions being very similar to the one used in the present study. The difference between the value 1.4 nm deduced for  $\xi_0$  from the present analysis and the value  $\xi_0 = 3.27$  nm, reported in Ref. [9], can be explained as follows. In  $C_{12}E_5 + H_2O$  solutions, the radius  $R_1$  of the monomer is large, and is about two times  $\xi_0$ , leading to a very strong influence of the cutoff parameter in Eqs. (11) and (12). In such circumstances and in the hydrodynamic regime, the droplet model predicts an upward curvature for the double logarithmic plot of the intensity as a function of  $\epsilon$ , in agreement with the experimental data. Such a behavior is not explained by the OZ formula which predicts in this regime that this plot should be a straight line of slope  $\gamma$ . However, this curvature can be accounted for by adding phenomenologically a large constant static background to the OZ formula. This background has in turn a strong influence on the apparent values of this indices  $\gamma$  and  $\nu$ , and also on  $\xi_0$ . Using this procedure leads to values of  $\gamma$  and  $\nu$  lower than their corresponding universal values ( $\gamma = 1.239$ ,  $\nu = 0.63$ ), in agreement with the numerical results reported in Ref. [9].

As far as dynamical critical phenomena are concerned, introducing dynamical background effects strongly improves the fit to the experimental results. However, some features we observed in the hydrodynamic regime cannot be explained. Indeed the dynamical background produces an upward curvature of the log-log plot of  $\Gamma$  as a function of  $\epsilon$ , whereas the experiment shows a downward curvature, as in the case of a microemulsion system [22]. Therefore it is clear that classical theories of critical phenomena cannot accurately account for the experimental results we report. On the other hand, the modified version of the dynamical droplet model very well accounts for all of our experimental results in the entire temperature and wave-vector range investigated here, suggesting universality both in the critical exponents and in the amplitude ratio. We therefore believe that the apparently too small values of the exponents  $\gamma$  and  $\nu$  previously reported [9] are probably not connected to a breakdown of universality of critical phenomena, but more likely linked to an oversimplification of the classical theories which do not account accurately for the finite size of the monomer,

as shown in our earlier work [23]. This happens typically when  $R_1$  is of the order of a few nanometers and larger than  $\xi_0$ .

As concluding remarks, let us briefly discuss problems that are still open. One of the main difficulties encountered in the study of critical phenomena in the mixture  $C_{12}E_5 + \text{water}$  is to establish precisely the location of the critical point. The very detailed experimental study of the phase diagram of the present system we performed allowed us to set the critical composition to be  $C_c \simeq 12$  mg/g. At this composition the volume equality between the dilute and concentrated coexisting phases was also confirmed at a few mK above  $T_c$ . In addition, we obtained the phase-separation temperature by observing the onset of the so-called spinodal ring formed by the forward light scattered from the mixture. This spinodal-like ring was actually observed for the entire range of concentrations employed in this work. We reported [52] the phase diagram thus obtained for the present system, in which it appeared that the binodal could be much closer to the so-called spinodal. Schmid and Blossey [53] have suggested that the presence of an internal structure in a fluid may shrink the metastability region of the phase diagram, resulting in a spinodal line approaching the binodal. If this effect should occur in our case, it would be difficult to observe a temperature difference between the off-critical phase-separation and critical phase-separation temperatures. Therefore we do not rule out completely the fact that the sample at composition  $C = 12.0$  mg/g may not be exactly at the critical concentration. Indeed even if this composition is not exactly the critical one, the results given in this work should in fact remain valid. The observed properties associated with anomalous behavior along an off-critical isoconcentration near the critical point should be nearly the same as along the critical isoconcentration, when accounting for a slight difference in the temperature  $T_{sp} - T_c$ .

It is worthwhile to point out also that micellar solutions are in general quite sensitive to shear flow, giving rise to significant nonlinear effects. These effects sometimes tend to produce differences in the effective viscosity measured under shearing, depending on the types of viscometers employed. As an example, using a capillary-tube viscometer we have estimated typical viscosity values of about 2.3–2.4 mPa s, while in the present analysis the value of  $\eta \simeq 2.2$  mPa s at  $\epsilon \sim 2 \times 10^{-3}$  has been used. By considering the possibly large errors due to shear-induced nonlinear effects we infer that the maximum error of our critical viscosity could be about 10%, while the relative one remains within 1%. Therefore future studies should focus on the nonlinear effects in shearing to get precise knowledge of viscosity behavior in the present system.

In addition to the above problems, a general question must be addressed. Martinez-Mekler, Al-Noaimi, and Robledo [54] have suggested that in a micellar solution model a crossover due to temperature-dependent interactions may occur much closer to the critical temperature, leading to an unusual compression of the critical region and to effective exponents close to criticality, while

universality should always be preserved. They have pointed out that, depending on the mixture energy parameters, the interactions may change sign at a certain temperature  $T_0$ , very close to the  $T_c$ , resembling the so-called  $\Theta$  point for a macromolecular solution where the second virial coefficient vanishes. It has also been recognized experimentally by Fujimatsu *et al.* [55] that the  $\Theta$  point associated with a micellar solution may be located at a temperature slightly below  $T_c$ . Their suggestions are quite attractive as a possible explanation for the unexpected behaviors observed very close to  $T_c$ . Unfortunately, it is not possible to conclude whether the present system behaves as the micellar solution model proposed by Martinez-Mekler, Al-Noaimi, and Robledo [54], although the unusual leveling off experimentally observed in the critical behavior of the  $C_{12}E_5$  mixture would appear to conform to their suggestions.

#### ACKNOWLEDGMENTS

We are indebted to M. Matsuno and T. Enomoto for valuable experimental assistance. In addition, we have benefited from discussions with Professor F. Tanaka, Professor H. Ushiki, and Professor T. Yamamoto, who provided crucial insights into the interpretation of our experiments through this work. The research at Gunma University was supported by the Japanese Ministry of Education, Science and Culture under Grant No. 02640271. J.R. would like to thank JSPS and CNRS for supporting his stay at Gunma University during which part of this work was completed. P.T. gratefully acknowledges support from GNSM-CNR and INFN-MURST. Centre de Physique Moléculaire Optique et Hertzienne is Unité Associée 283 du Centre National de la Recherche Scientifique.

- 
- [1] M. Corti and V. Degiorgio, *Phys. Rev. Lett.* **55**, 2005 (1985); V. Degiorgio, in *Physics of Amphiphiles, Micelles, Vesicles and Microemulsions*, edited by V. Degiorgio and M. Corti (North-Holland, Amsterdam, 1985).
- [2] A. M. Belloq, in *Micelles, Membranes, Microemulsions, and Monolayers*, edited by W. M. Gelbart, A. Ben-Shaul, and D. Roux (Springer-Verlag, New York, 1994), p. 521.
- [3] A. M. Belloq, P. Honorat, and D. Roux, *J. Phys. (Paris)* **46**, 743 (1985).
- [4] R. Strey and A. Pakusch, in *Surfactant in Solution*, edited by K. L. Mittal and P. Bothorel (Plenum, New York, 1987), Vol. 4.
- [5] G. Dietler and D. S. Cannell, *Phys. Rev. Lett.* **60**, 1852 (1989).
- [6] J. P. Wilcoxon, D. W. Schaefer, and E. W. Kaler, *J. Chem. Phys.* **90**, 1909 (1989); J. P. Wilcoxon and E. W. Kaler, *Phys. Rev. Lett.* **60**, 333 (1988); *J. Chem. Phys.* **86**, 4684 (1987).
- [7] K. Hamano, N. Kuwahara, I. Mitsushima, K. Kubota, and T. Kamura, *J. Chem. Phys.* **94**, 2172 (1991); K. Hamano, N. Kuwahara, K. Kubota, and I. Mitsushima, *Phys. Rev. A* **43**, 6881 (1991).
- [8] For a review, see P. C. Hohenberg and H. I. Halperin, *Rev. Mod. Phys.* **49**, 435 (1977).
- [9] K. Hamano, T. Sato, T. Koyama, and N. Kuwahara, *Phys. Rev. Lett.* **55**, 1472 (1985).
- [10] K. Hamano, N. Kuwahara, T. Koyama, and S. Harada, *Phys. Rev. A* **32**, 3168 (1985).
- [11] M. E. Fisher, *Phys. Rev. Lett.* **57**, 1911 (1986).
- [12] L. Reatto, *Nuovo Cimento D* **8**, 497 (1986).
- [13] C. Bagnuls and C. Bervillier, *Phys. Rev. Lett.* **58**, 435 (1987).
- [14] P. G. Nilson, H. Wennerstrom, and B. Lindman, *J. Phys. Chem.* **78**, 2025 (1983).
- [15] For example, see G. J. T. Tiddy, *Phys. Rep.* **57**, 1 (1980).
- [16] J. Rouch, P. Tartaglia, A. Safouane, and S. H. Chen, *Phys. Rev. A* **40**, 2013 (1989); J. Rouch, A. Safouane, P. Tartaglia, and S. H. Chen, *J. Chem. Phys.* **90**, 3756 (1989).
- [17] D. W. Oxtoby and W. M. Gelbart, *J. Chem. Phys.* **61**, 3157 (1974).
- [18] For example, see D. J. T. Tiddy, L. Waring, T. Bostock, and P. McDonald, *J. Chem. Soc. Faraday Trans. 1* **79**, 975 (1983).
- [19] D. Blankschtein, G. M. Thurston, and G. B. Benedek, *Phys. Rev. Lett.* **54**, 955 (1985); *J. Chem. Phys.* **85**, 7268 (1986).
- [20] K. Kawasaki, *Ann. Phys. (N.Y.)* **61**, 1 (1970); K. Kawasaki, in *Phase Transitions and Critical Phenomena*, edited by C. Domb and M. S. Green (Academic, New York, 1976), Vol. 5A, p. 165.
- [21] H. C. Burstyn, J. V. Sengers, J. K. Bhattacharjee, and R. A. Ferrell, *Phys. Rev. A* **28**, 1567 (1983).
- [22] P. Tartaglia, J. Rouch, and S. H. Chen, *Phys. Rev. A* **45**, 7257 (1992); J. Rouch, P. Tartaglia, and S. H. Chen, *Phys. Rev. Lett.* **71**, 1947 (1993).
- [23] E. Ducros, J. Rouch, K. Hamano, P. Tartaglia, and S. H. Chen, *J. Phys.: Condens. Matter* **6**, A293 (1994); E. Ducros, S. Haouache, J. Rouch, K. Hamano, K. Fukuhara, and P. Tartaglia, *Phys. Rev. E* **50**, 1291 (1994).
- [24] C. M. Sorensen, B. J. Ackerson, R. C. Mockler, and W. J. O'Sullivan, *Phys. Rev. A* **13**, 1593 (1976).
- [25] J. E. Martin and B. J. Ackerson, *Phys. Rev. A* **31**, 1180 (1985); J. E. Martin, J. Wilkonson, and D. Adolf, *ibid.* **36**, 1803 (1987); J. E. Martin, J. Wilkonson, and J. Odinek, *ibid.* **43**, 585 (1991).
- [26] A. Coniglio and W. Klein, *J. Phys. A: Math. Gen.* **13**, 2775 (1980).
- [27] D. Stauffer, in *On Growth and Form*, edited by H. E. Stanley and N. Ostrowsky (Martinus Nijhoff, Dordrecht, 1986); D. Stauffer and A. Aharony, in *Introduction to Percolation Theory* (Taylor and Francis, London, 1992); D. Stauffer, *Phys. Rep.* **54**, 1 (1979); Y. Gefen, A. Aharony, B. Mandelbrot, and S. Kirkpatrick, *Phys. Rev. Lett.* **47**, 1771 (1981).
- [28] P. Guenoun, F. Perrot, and D. Beysens, *Phys. Rev. Lett.* **63**, 1152 (1989).
- [29] D. Beysens, P. Guenoun, and F. Perrot, *J. Phys.: Condens. Matter* **2**, SA127 (1990).
- [30] K. Hamano, S. Yamashita, and J. V. Sengers, *Phys. Rev. Lett.* **68**, 3579 (1992).

- [31] J. P. Wilcoxon, *J. Phys. Chem.* **94**, 7587 (1990).
- [32] C. A. Tracy and B. M. McCoy, *Phys. Rev. B* **12**, 75 (1974).
- [33] M. E. Fisher, *Physica* **28**, 172 (1962); *J. Math. Phys.* **5**, 944 (1964).
- [34] J. G. Shanks and J. V. Sengers, *Phys. Rev. A* **38**, 885 (1988).
- [35] R. A. Ferrell and J. K. Bhattacharjee, *Phys. Rev. A* **19**, 348 (1979), and references therein.
- [36] K. Hamano, M. Tachikawa, Y. Kenmochi, and N. Kuwahara, *Phys. Lett.* **90A**, 425 (1982); N. Kuwahara, M. Tachikawa, K. Hamano, and Y. Kenmochi, *Phys. Rev. A* **25**, 3449 (1982); N. Kuwahara, K. Hamano, and T. Koyama, *ibid.* **32**, 1279 (1985).
- [37] K. Hamano, T. Kawazura, T. Koyama, and N. Kuwahara, *J. Chem. Phys.* **82**, 2718 (1985), and references therein.
- [38] K. Hamano, T. Ishii, M. Ozawa, J. V. Sengers, and A. H. Krall, *Phys. Rev. E* **51**, 1254 (1995).
- [39] E. Brezin and D. J. Wallace, *Phys. Rev. Lett.* **28**, 591 (1972); P. Schofield, J. D. Litster, and J. T. Ho, *ibid.* **23**, 1098 (1969); J. T. Ho and J. D. Litster, *Phys. Rev. B* **2**, 4523 (1970).
- [40] H. Seto, E. Yokoi, S. Komura, D. Schwahn, K. Mortensen, J. Suzuki, M. Ohnuma, and Y. Ito, *J. Phys. (France) IV* **3**, 161 (1993).
- [41] S. H. Chen and J. Teixeira, *Phys. Rev. Lett.* **57**, 2583 (1986).
- [42] K. Hamano, N. Kuwahara, B. Chin, and K. Kubota, *Phys. Rev. A* **43**, 1054 (1991).
- [43] R. Perl and R. A. Ferrell, *Phys. Rev. Lett.* **29**, 51 (1972); *Phys. Rev. A* **6**, 2358 (1972).
- [44] H. C. Burstyn and J. V. Sengers, *Phys. Rev. A* **27**, 1071 (1983).
- [45] J. V. Sengers, *Int. J. Thermophys.* **5**, 805 (1985).
- [46] K. Hamano, T. Kaneko, K. Fukuhara, and N. Kuwahara, *Int. J. Thermophys.* **10**, 389 (1989); K. Hamano, N. Kuwahara, I. Mitsushima, K. Kubota, and J. Ito, *Phys. Lett. A* **150**, 405 (1990).
- [47] A. Onuki and K. Kawasaki, *Ann. Phys. (N.Y.)* **121**, 456 (1979); *Suppl. Prog. Theor. Phys.* **64**, 436 (1978); A. Onuki, K. Yamazaki, and K. Kawasaki, *Ann. Phys. (N.Y.)* **131**, 217 (1981).
- [48] G. A. Olchowy and J. V. Sengers, *Phys. Rev. Lett.* **61**, 15 (1988); P. C. Albright, J. V. Sengers, J. F. Nicoll, and M. Ley-Koo, *Int. J. Thermophys.* **7**, 75 (1986); Z. Y. Chen, A. Abbaci, S. Tang, and J. V. Sengers, *Phys. Rev. A* **42**, 4470 (1990).
- [49] J. M. di Meglio, L. Paz, M. Dvolaitzky, and C. Taupin, *J. Phys. Chem.* **88**, 6036 (1984).
- [50] W. Brown, Z. Pu, and R. Rymden, *J. Phys. Chem.* **92**, 4466 (1988).
- [51] M. Corti, C. Minero, and V. Degiorgio, *J. Phys. Chem.* **88**, 309 (1984).
- [52] K. Hamano, T. Koyama, and N. Kuwahara, *Rep. Prog. Polym. Phys. Jpn.* **27**, 471 (1984).
- [53] F. Schmid and R. Blossey (unpublished).
- [54] G. Martinez-Mekler, G. F. Al-Noaimi, and A. Robledo, *Phys. Rev. A* **41**, 4513 (1990).
- [55] H. Fujimatsu, K. Takagi, M. Matsuda, and S. Kuroiwa, *J. Colloid Interface Sci.* **94**, 237 (1983).